Passive Intermodulation of Analog and Digital Signals on Transmission Lines With Distributed Nonlinearities: Modelling and Characterization

Dmitry S. Kozlov, *Student Member, IEEE*, Alexey P. Shitvov, *Member, IEEE*, Alexander G. Schuchinsky, *Fellow, IEEE*, and Michael B. Steer, *Fellow, IEEE*

***Abstract*— Passive intermodulation (PIM) often limits the performance of communication systems with analog and digitally modulated signals and especially of systems supporting multiple carriers. Since the origins of the apparently multiple physical sources of nonlinearity causing PIM are not fully understood, the behavioral models are frequently used to describe the process of PIM generation. In this paper, a polynomial model of memoryless nonlinearity is deduced from PIM measurements of a microstrip line with distributed nonlinearity with two-tone CW signals. The analytical model of nonlinearity is incorporated in Keysight Technology's ADS simulator to evaluate the metrics of signal fidelity in the receive band for analog and digitally modulated signals. PIM-induced distortion and cross-band interference with modulated signals are compared with those with two-tone CW signals. It is shown that conventional metrics can be applied to quantify the effect of distributed nonlinearities on signal fidelity. It is found that the two-tone CW test provides a worst-case estimate of cross-band interference for two-carrier modulated signals, whereas, with a three-carrier signal, PIM interference in the receive band is noticeably overestimated. The simulated constellation diagrams for QPSK signals demonstrate that PIM interference exhibits the distinctive signatures of correlated distortion and this indicates that there are opportunities for mitigating PIM interference and that PIM interference cannot be treated as noise. One of the interesting results is that PIM distortion on a transmission line results in asymmetrical regrowth of output PIM interference for modulated signals.**

***Index Terms*— Cross-band interference, distributed nonlinearity, intermodulation distortion (IMD), memoryless polynomial model, passive intermodulation (PIM), signal integrity.**

I. Introduction

In WIRELESS communications, intermodulation (IM) distortion is broadly defined as the appearance of additional spectral components, i.e., spectral regrowth, at the output of a nonlinear system that are distinct from the carrier frequencies of input signals and their integer multiples. IM is usually a harmful effect, as the spurious spectrum generated by the transmitted signals may overlap that of received signals in a transceiver front-end. Such co-site interference can cause strong cross-band interference and receiver desensitization and can even render the whole link inoperable [1]. This is a problem in advanced LTE systems which support carrier aggregation in mobile units where fewer resources are available to minimize the sources of PIM through overdesign.

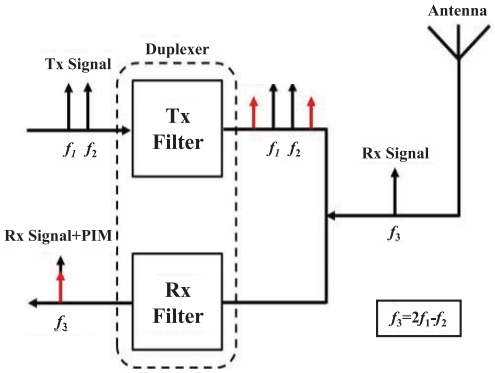

Fig. 1. Schematic diagram of cross-band PIM in a BS antenna duplexer.

The sources of nonlinear interference in communication systems are diverse, but a power amplifier (PA) is usually regarded as a primary source of adjacent transmit (Tx) channel interference. While the out-of-band spectrum can be efficiently rejected by high-performance Tx filters, a bandpass filter itself, as well as power combiners, phase shifters, and beamforming networks in a base station (BS), can cause strong cross-band interference due to passive intermodulation (PIM) of modulated carriers. Fig. 1 shows a schematic diagram of PIM occurrence in generic BS front-end and antenna. The third-order PIM products of frequency $f_3 = 2f_1 - f_2$, generated by weak nonlinearities of the Tx filter and antenna operated with two high-power carriers of frequencies f_1 and f_2, fall into the receive (Rx) band and distort weak received signals of frequency f_3. This results in receiver desensitisation, reduced signal-to-noise ratio (SNR), and degraded channel capacity.

Primary sources of PIM are located in the circuit components shared by the transmit and receive signals such as the transmissions lines and antenna on the antenna-side

Manuscript received November 1, 2015; revised January 19, 2016, March 28, 2016 and March 30, 2016; accepted March 30, 2016. This work was supported by FP7 Marie Curie ITN ARTISAN under Grant 316426. The work of D. Kozlov was supported by the FP7 Marie Curie ITN project ARTISAN. This paper is an expanded version from IEEE MTT-S International Workshop on Integrated Nonlinear Microwave and Millimetre-wave Circuits, Taormina, Italy, October 2015.

D. S. Kozlov, A. P. Shitvov, and A. G. Schuchinsky are with the Institute of Electronics, Communications and Information Technology, Queen's University Belfast, BT3 9DT, U.K. (e-mail: d.kozlov@qub.ac.uk; a.shitvov@qub.ac.uk; a.g.schuchinsky@gmail.com).

M. B. Steer is with the Department of Electrical and Computer Engineering, North Carolina State University, Raleigh, NC 27695 USA (e-mail: mbs@ncsu.edu).

Color versions of one or more of the figures in this paper are available online at http://ieeexplore.ieee.org.

Digital Object Identifier 10.1109/TMTT.2016.2550046

of the duplexer. Therefore, signal pre-distortion used for linearization of power amplifiers cannot eliminate PIM interference generated by the passive devices. Mitigation of the PIM impact is complicated by the presence of several nonlinearities of diverse physical nature which are difficult to identify and discriminate using existing measurement techniques. Only a mechanism with a unique signature, the electro-thermal resistive effect, has been consistently defined so far [2]. This necessitates the need to use behavioral models for PIM characterisation, and these models require validation for particular situations.

Current approaches to assessing the PIM performance of antennas, passive components (e.g., filters, multiplexers and phase-shifters), circuit boards and communications payloads are incorporated in various communication and radar standards. The commonly used technique is a two-tone continuous wave (CW) test, specified by IEC62037–1 (2012) standard [3]. The test involves scalar measurements of the power levels of PIM products of the third or higher orders in the receive (Rx) band generated due to mixing of two transmitted (Tx) carriers of specified discrete frequencies as illustrated in Fig. 1. For example, a typical pass/fail threshold for the third-order PIM (PIM3) products generated by a BS antenna is specified as -112 dBm with two 43 dBm discrete CW carriers. This PIM level is commensurate with the thermal noise power of -114 dBm in 1 MHz bandwidth. Swept carrier frequency measurements are also used to monitor PIM variations across Rx band. Some commercial PIM analyzers support swept carrier power measurements but such tests are rarely used in practice. The merits and limitations of the standard two-tone CW PIM tests were discussed in [4] in the context of cable assemblies and connectors. However, adequacy and utility of PIM characterisation with two discrete CW tones, which is cost effective as compared to using wideband modulated signals and multiple tones, requires further investigation and justification now when there are many concurrent carriers and protocols with high peak-to-mean envelope ratios (PMEPR).

It used to be tacitly assumed that the PIM effect would not depend on the signal type and could be assessed using the two-tone CW models and respective tests. However, there is increased concern in industry about the suitability of the current PIM tests for emerging broadband multicarrier systems that support diverse modulation schemes and the legacy standards, see, e.g., [5]–[7]. Furthermore, carrier aggregation in cost-constrained mobile handsets places increased emphasis on modelling to aid in the design of systems with controlled and predictable levels of PIM. At the same time, signal waveforms become increasingly complicated, and, together with multiple carriers, the PMEPR of combined signals and peak powers can be very large. Therefore, representative signal integrity metrics are now required to capture the essential dynamics of PIM distortion, which could be used for efficient digital correction of the received signals. Correlation analysis techniques are extensively applied to characterization of the in-band and adjacent channel nonlinear distortions in active devices and circuits, [8]–[10]. However, cross-band PIM interference caused by complex modulated signals transmitted through passive components of a Tx chain is still lacking metrics beyond that based on ideal-mixer models. Thus PIM interference is commonly treated as uncorrelated noise. Alternatively, if the essential dynamics of signal distortion by PIM interference is incorporated into representative signal fidelity metrics, the effect of PIM distortion of received signals could be mitigated with the aid of efficient digital correction of received signals.

This paper focuses on modelling PIM interference generated by the distributed nonlinearities of transmission lines (TLs) carrying modulated signals. The PIM simulation concepts for these structures with two-tone CW carriers have been discussed in [2], [11]–[18], and here we develop a behavioral model retrieved from the results of two-tone PIM tests and show that this model can be used for the prediction of PIM distortion of modulated signals on a TL with distributed nonlinearity (TLDN) employed in circuit boards and antenna feeds. The PIM effect in the presence of analog and digitally modulated signals is examined in terms of the commonly used metrics of signal integrity and adjacent channel power ratio deduced from two-tone CW PIM tests. This paper significantly extends and elucidates the modeling concept outlined in the conference summary [11]. In particular, we employ here a novel analysis based on a polynomial model of nonlinearity and suggest an advanced characterization approach. The new results are presented, including those related to the model extraction and simulations of PIM distortion of digital signals.

In Section II, an analytical single-input single-output model of two-tone IM generation in a nonlinear network is revisited, and closed-form expressions for PIM products are obtained and related to interference metrics. In Section III, the model is extended to a TLDN, and its parameters are extracted from PIM3 measurements on a microstrip line and subsequently validated. In Section IV, the model of nonlinearity is used in envelope tracking simulations to assess distortions of analog and digitally modulated signals by PIM products generated on the TL. The simulation results for modulated signals are compared with the results of two-tone CW tests using the standard signal integrity metrics. The effects of PIM interference on analog and digitally modulated signals and the suitability of the two-tone CW PIM test for assessment of modulated signals are discussed in the conclusion.

II. PIM Generation by Passive Nonlinearity

PIM generation by nonlinear mixing of high-power signals is revisited here by considering a memoryless nonlinear device described by a polynomial transfer function (TF). The choice of the model is informed by our experimental studies of PIM generation in printed lines. The results of our measurements in power/frequency sweep modes have shown that a phenomenological memoryless model adequately describes the processes of frequency mixing by a passive nonlinearity on a transmission line. The model, in principle, can be extended to a Hammerstein–Wiener model to include memory effects, but its identification is not possible by conventional PIM testing.

In real-world two-port circuits, PIM products generated inside a passive component appear at its output and input ports as the “forward” and “reverse” (also known as “reflected”) PIM products, respectively. For the sake of clarity, the analysis below is limited to the PIM products of odd orders, which fall

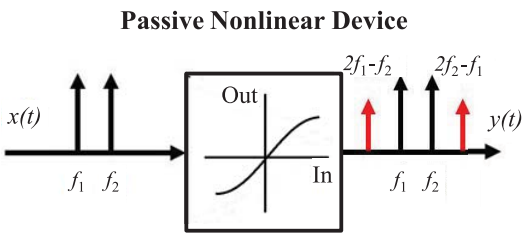

Fig. 2. Block diagram of the model structure.

in adjacent Rx band and so are dominant contributors to cross-band interference and Rx signal distortion. Generalization to a full polynomial TF is straightforward and is not presented here for brevity. In the discussion below, we refer to intermodulation (IM) phenomena, since the presented formalism is equally applicable to both active and passive nonlinearities.

Consider the passive weakly nonlinear device shown schematically in Fig. 2. Its nonlinear TF maps an input two-tone modulated signal $x(t)$ onto an output waveform $y(t)$ which contains the carriers' harmonics and IM frequencies. The input two-tone signal is represented by the form

$$x(t) = A_1(t)\cos[\omega_1 t + \theta_1(t)] + A_2(t)\cos[\omega_2 t + \theta_2(t)] \quad (1)$$

where $A_{1,2}(t)$ and $\theta_{1,2}(t)$ are the modulation amplitude (AM) and phase (PM), respectively, and $\omega_{1,2} = 2\pi f_{1,2}$ are carrier frequencies, and it is assumed that $\omega_1 < \omega_2$.

For the analysis of the odd-order IM products, the TF of a memoryless weak nonlinearity can be described by an odd-order polynomial of power N as

$$\begin{aligned} y(t) &= a_1 x(t) + a_3 x^3(t) + \cdots + a_N x^N(t) \\ &= \sum_{n=0}^{(N-1)/2} a_{2n+1} x^{2n+1}(t) \end{aligned} \quad (2)$$

where, without loss of generality, coefficients $a_1, a_3, \ldots, a_N$ are assumed to be real-valued and time-invariant. It is necessary to note that the polynomial approximation (2) of the nonlinear TF represents a large-signal model of a passive nonlinear device which is symmetrical for the positive and negative voltages. However, when the nonlinearity is associated with nonsymmetrical junctions at the microscopic scale, even-order terms need to be included in the polynomial expansion of the TF. Various models of lumped and distributed passive nonlinearities have been reported in the literature, e.g., for the limiter-type [19], hysteretic [20], dynamic transmission line [21] nonlinearities, and tunnelling currents in MIM contacts [22]. An optimal model of the actual nonlinearity is determined by the specific physical mechanisms, but their discussion is beyond the scope of this paper.

For the input signal $x(t)$ of the type shown in (1), the output waveform $y(t)$ in (2) can be obtained in a closed form as detailed in Appendix A. Since the odd-order IM products closest to the carrier bands are usually stronger and often appear in the Rx bands, it is instructive to consider them in more detail using their explicit expressions (A9) for the identical envelops of the carriers with $A_1(t) = A_2(t) = A(t)$ and $\theta_1(t) = \theta_2(t) = \theta(t)$.

In the case of CW signals, the spectrum of the output waveform contains components at the carrier frequencies, lower and upper sideband odd order IM frequencies, and odd harmonics of the carrier frequencies. In our analytical model, the output spectrum is truncated to retain only the fundamental frequencies in the Tx band and the odd-order IM products in the immediately adjacent and alternate bands, thus excluding all harmonics and higher-order IM products. The odd-order IM frequencies closest to the carriers' band satisfy the following condition:

$$\omega_l = (l+1)\omega_1 - l\omega_2 \quad (3)$$

where $l = (M-1)/2$, and $|M|$ is the order of the IM product, $M = \pm 3, \pm 5, \ldots, \pm N$. The positive values of M correspond to the lower sideband IM products, whereas the negative values to the upper sideband IM products. The respective bandlimited output waveform can be expressed in the following form:

$$\hat{y}(t) = \mathrm{Re}\left\{ \sum_{\substack{M=-N \\ M-odd}}^{N} y_M(t) \mathrm{e}^{j[(M+1)/2\ \omega_1 - (M-1)/2\ \omega_2]\cdot t} \right\} \quad (4)$$

where

$$\begin{aligned} y_M(t) = \mathrm{e}^{j\theta(t)} &\sum_{n=0}^{(N-1)/2} \frac{a_{2n+1}}{2^{2n+1}} \binom{2n+1}{n+1} A^{2n+1}(t) \\ &\times \sum_{k=(M+1)/2}^{n+1} \binom{n+1}{k} \binom{n}{k-\frac{M+1}{2}} \end{aligned} \quad (5)$$

and $y_M(t)$ represents the baseband envelope of the carriers and IM products at the device output. For example, $M = 3$ corresponds to the third-order IM (IM3) product in the lower sideband, which usually overlaps with the Rx band, and its baseband envelope is given by $y_3(t)$ in (5). It is also necessary to remark that the baseband envelopes of the carriers, corresponding to $M = \pm 1$, exhibit distortion due to depletion in nonlinear mixing.

The utility of the closed-form expressions (4) and (5) cannot be overstated. They enable the spectral-correlation analysis of the cross-band IM interference. When applied to additive white Gaussian noise (AWGN), or other noise-like test signals, the terms in (4) can be orthogonalized to discriminate the correlated and uncorrelated noise terms, similarly to [8], and to enable development of efficient linearization and detection algorithms. At the same time, the analytical relations obtained here provide fairly accurate initial approximations for more detailed numerical analysis of the IM products generated by complex signals when using harmonic balance-based simulation tools.

To quantify the appearance of spurious spectral components arising in the Rx band due to the nonlinear mixing of the input signals in the Tx band, it is expedient to use the adjacent band power ratio (ABPR) metric, [23]. The ABPR is defined as the ratio of the mean power of spurious emission in the Rx band in the absence of the received signal from antenna, to the

transmitter mean power over the Tx band, viz.

$$\text{ABPR} = \frac{\sum_{Rx} |\hat{Y}(f)|^2}{\sum_{Tx} |X(f)|^2} \tag{6}$$

where $X(f)$ and $\hat{Y}(f)$ are the Fourier transforms of the Tx input signal, $x(t)$, and the band-limited output signal, $\hat{y}(t)$, accrued over the Tx and Rx band, respectively. Hence, the output Rx spectrum contains all odd-order IM products defined by (4) that fall inside the Rx frequency band. The ABPR metric proved to be convenient for the assessment of distortion for both discrete-tone and modulated signals. It is also directly related to the dBc measure in the standard two-tone CW PIM test, where the input power per carrier is just 3 dB lower than the Tx power in the denominator of (6). Using the nonlinear TF expansions in (4) and (5), the ABPR can be calculated analytically for a two-tone input signal, once the coefficients a_n in (2) are determined. In the next section, the polynomial model (2) is extracted from the two-tone scalar PIM measurements in the power sweep mode.

III. Polynomial Model for PIM Analysis of TLDN

The PIM characterization at variable power and frequency of carriers is necessary for identifying distinctive signatures of the dominant nonlinearity. The PIM measurements with swept power, which are somewhat similar to those for a memoryless PA, see, e.g., [24], enable us to deduce a polynomial approximation (2) of the nonlinear TF at a given frequency. Then using the frequency sweep data, the polynomial coefficients in (2) can be made frequency-dependent. However, frequency variations of the polynomial coefficients are normally very small across the specified band and commensurate with overall uncertainty of fitting the data to the polynomial model (2). Therefore, the use of constant polynomial coefficients proved to be sufficient for PIM performance assessment as demonstrated next.

A. Polynomial Model for PIM3 on a Microstrip Line

Retrieval of the polynomial coefficients in (2) from power sweep measurements of PIM3 is illustrated here for a printed microstrip TL [25]. The test specimens of straight uniform microstrip lines of width $W = 1.9$ mm and different lengths were fabricated on a single panel of custom-built Taconic TLG-30 PCB material ($\varepsilon_r = 3.0, \tan\delta = 0.0026$, substrate thickness $h = 0.76$ mm), which exhibits fairly strong nonlinearity of the dielectric substrate. The PCB material TLG-30 is not qualified for BS antenna applications, and it was used in our studies only for the purpose of the effect demonstration and model verification. The PCB layout, test fixtures, and the measurement setup are detailed in Appendix B.

Forward PIM3 products of frequency 910 MHz (carrier frequencies $f_1 = 935$ MHz and $f_2 = 960$ MHz) generated on a reference microstrip line of length $L_0 = 914$ mm were measured with a commercial Summitek SI-900B PIM analyzer for a range of carrier powers from 24 to 44 dBm. The acquired data were fitted to the polynomial model (2) by minimizing the residual root mean square error (RMSE).

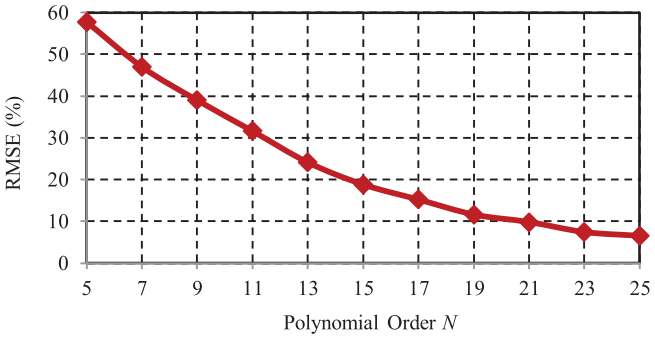

Fig. 3. RMSE of the measurement data fitting with the polynomial approximation (2) by least mean square algorithm versus the polynomial order, N.

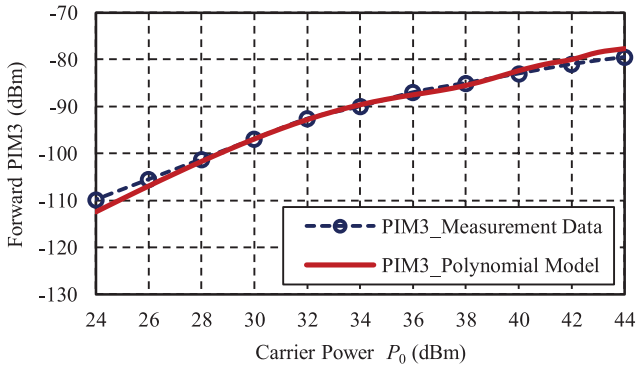

Fig. 4. Comparison of the measured [25] and simulated PIM3 products at the sweep carrier power, P_0 at polynomial order $N = 23$.

The RMSE convergence versus the polynomial order N is shown in Fig. 3.

It shows that retaining 12 nonzero odd-order terms ($N = 23$) in (2) yields a fitting error less than 8% and account for the next non-zero term ($N = 25$) reduces the error by less than 1%. The PIM3 products simulated with the retrieved polynomial coefficients a_n for $N = 23$ (see Appendix C) are juxtaposed with the measurement data in Fig. 4. Their comparison for broad range of carrier power shows good agreement. The model accuracy could be further improved by using the PIM3 data of independent power sweeps of each carrier [25].

The polynomial coefficients a_n deduced from the two-tone PIM3 measurements on the reference microstrip TL of length $L_0 = 914$ mm were used for evaluating the forward PIM products on TLs of other lengths. As observed in our previous studies [26], forward PIM3 monotonically grows with TL length, L, owing to the close phase matching between the PIM3 products and carriers. This suggests that the coefficients a_n can be nearly linearly scaled in order to simulate the effect of the transmission line length. Taking also into account attenuation of both the carriers and PIM products due to the losses, the $a_n(L)$ dependence can be approximated as follows:

$$a_n(L) = \left[\frac{L}{L_0}\right]^{1-\alpha} a_n(L_0) \tag{7}$$

where α represents the attenuation parameter which is obtained by fitting the simulated PIM3 products with the coeffi-

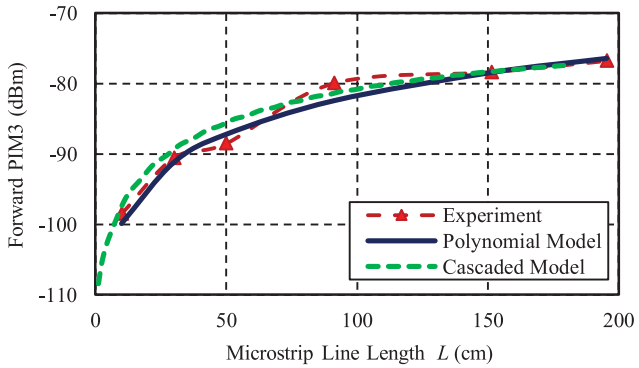

Fig. 5. Comparison of the simulated (polynomial model (2)–(7) and cascaded model [27]) and measured ([26]) PIM3 products over the range of transmission line lengths.

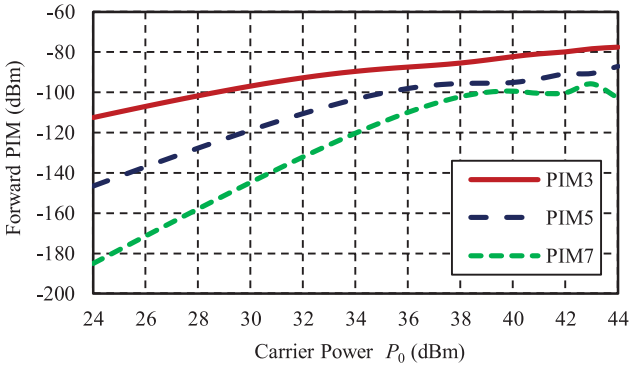

Fig. 6. Third-, fifth-, and seventh-order PIM products on the reference microstrip TL simulated by the polynomial model in the range of carrier power values.

cients $a_n(L_0)$ from Appendix C to the measurement data [26] for TLs of different lengths. Fig. 5 shows that the PIM3 products simulated over a range of TL lengths with $\alpha = 0.1$ are in fairly good agreement with the measurements at variable L.

In order to further verify validity of the scalable polynomial coefficients $a_n(L)$, a TL network with distributed nonlinearity was simulated in Keysight Technology's ADS simulator and compared with the polynomial model (2). The TLDN was modelled as a cascade of electrically short segments each described by an *RLC* circuit with third-order capacitive nonlinearity, [18], [27]. The model was found to be sufficient for a fixed carrier power level. The capacitive nonlinearity was deduced from the experimental data. The TLDN was analyzed using the formalism of X-parameters in ADS [28]. Fig. 5 shows that the PIM3 characteristics calculated using the polynomial model (2) with scalable coefficients $a_n(L)$ fully agree with both the ADS simulations and measurements. This confirms that the forward-traveling PIM products generated at each point of the TL add up in phase and the output PIM level monotonically increases with the TLDN length and that it is adequately described by the polynomial model (2) with the scalable coefficients introduced in (7).

B. Higher Order PIM Products

The coefficients a_n of the polynomial model (2) used so far were deduced from PIM3 measurement data in the lower sideband only. Their applicability to the analysis of higher-order PIM products still needs further assessment. The simulated power sweep characteristics of the fifth and seventh order PIM products, which become increasingly important for the design of modern wideband communication systems, are shown in Fig. 6 for the reference TL, along with the third-order PIM products. All the plots, simulated with the same polynomial coefficients given in Appendix C, exhibit slopes which are in good qualitative agreement with the measurements of a 914 mm long matched nonuniform TL fabricated on the TLG-30 material in [25]. The quantitative discrepancy between the results in Fig. 6 and data in [25] is due to the different TL width.

Nonmonotonic behavior of the fifth- and seventh-order PIM products at the higher carrier power is attributed to insufficient order of the polynomial model of nonlinearity, as well as to a larger phase mismatch between the propagating carriers and higher-order PIM products. Further experimental studies are necessary to assess the accuracy of the nonlinear models retrieved from two-tone PIM3 measurements and the effect of the measurement uncertainties.

Finally, it is noteworthy that, as the magnitudes of higher-order PIM products become commensurable with PIM3, they should be duly accounted for in the ABPR metric (6), and this may require more terms in the polynomial model (2).

C. Applicability of the Polynomial Model of PIM

The polynomial approximation (2) is essentially a behavioral model of nonlinearity which is normally applicable only to lumped or discrete elements. Its coefficients a_n deduced from the measurement data allow comparative assessment of PIM performance without identifying the physical sources and causes of the nonlinear response. Although such models are sufficient for characterization of electrically small components, they are usually not applicable to distributed nonlinear structures with electrical size commensurate to wavelength. Nevertheless, it turns out that the polynomial model (2) adequately describes forward PIM products generated by distributed nonlinearities. For a microstrip TLDN this is achieved by introducing the length-dependent coefficients $a_n(L)$ given by (7). Such an extension of (2) is valid only when L is much shorter than the PIM *coherence length*, i.e., when the phase offset between the carriers and PIM products remains much less than π over the TL length, [16]. For reverse PIM products, the latter condition is met only if TLDN is shorter than half a wavelength, and a more elaborate model should be employed otherwise.

Alternatively, PIM generation in a TLDN could be simulated numerically with the aid of the ADS X-parameter solver, e.g., [18]. Then, making use of the TLDN equivalent circuit model with specified nonlinearity, both forward- and reverse-PIM products at the TLDN terminals can be efficiently calculated. However, this approach is far from being straightforward, because retrieval of the nonlinear equivalent circuit parameters from swept-power PIM3 measurement data is prone to slow convergence, and the harmonic balance solver

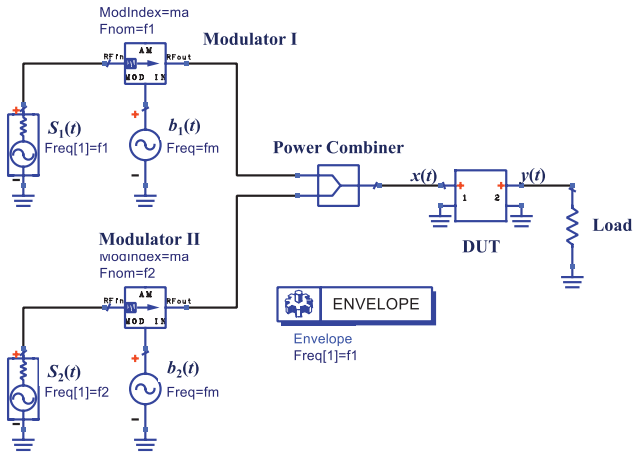

Fig. 7. Equation-based model for the study of cross-band interference caused by the passive TL nonlinearity employed in ADS Circuit Envelope solver.

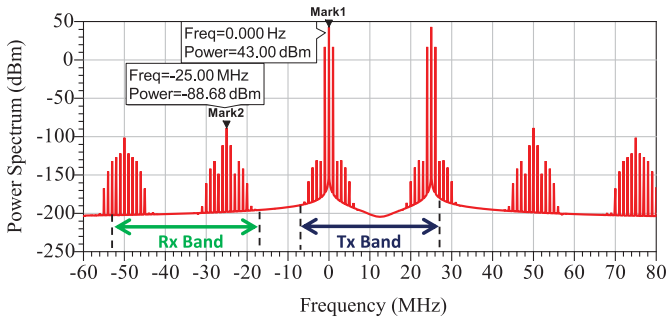

Fig. 8. Two-carrier AM signal spectrum at the TLDN output simulated for $m_a = 0.1$. The chart centre ("Mark 1") is at frequency 932.5 MHz.

becomes unstable for the multi-element higher order nonlinear cascaded networks. To alleviate the limitations of such direct numerical simulations, the polynomial model (2) with the extracted coefficients $a_n(L)$ has been incorporated in the ADS equation-based nonlinear analysis and applied to modelling PIM effects on modulated signals in circuits with distributed nonlinearities.

IV. PIM Effect on Modulated Signals

It was demonstrated in the preceding section that the polynomial model (2), retrieved from measured PIM3 data, adequately describes the weak nonlinearity of the TLDN and fairly accurately predicts PIM generation by two-tone CW signals. The purpose of this section is to explore the characteristics of PIM produced by the distributed passive nonlinearities of a transmission line for various numbers of modulated carriers and different types of modulation.

Once the model of nonlinearity has been defined, PIM distortion of analog and digitally modulated signals in the TLDN can be analyzed using the ADS Circuit Envelope solver. For this purpose, a length of TLDN is modelled as a cascade of electrically short sections using the simulation environment shown in Fig. 7, where DUT indicates a TLDN comprising its cascaded subsections. An analog test signal $x(t)$ is synthesized by mixing two CW carriers $S_{1,2}(t)$ modulated by signals $b_{1,2}(t)$. In the case of digital modulation, the baseband signals are properly conditioned using raised-cosine filters. An output signal $y(t)$ is described by the polynomial approximation (2) with the coefficients given in Appendix A.

It is necessary to note that while the polynomial model of a passive nonlinearity (2) is a memoryless model, it will be seen that the TLDN exhibits a memory-like effect associated with the phase coherence of carriers and PIM products. That is, the small relative growth in phase difference between carriers centered at different frequencies results in asymmetrical regrowth of output PIM interference for modulated signals. A similar asymmetry with amplifiers is attributed to baseband memory effects [29] but that is not the case here.

Thus, the memory-like effect inherent to PIM produced by a TLDN is distinct from that of the physical memoryless mechanism of nonlinearity itself. While in some circumstances the PIM generating mechanism can have baseband memory due to electro-thermal effects [2], [17], [30], this effect is not included in the model used here.

A. Amplitude Modulated Signals

First consider an input analog amplitude modulated (AM) test signal of the form

$$x(t) = A \cdot [1 + m_a \sin(\omega_m t)] \cdot [\cos(\omega_1 t) + \cos(\omega_2 t)] \quad (8)$$

where m_a is the modulation index, $\omega_{m,1,2} = 2\pi f_{m,1,2}$ and f_m is the modulation frequency, and f_1 and f_2 are carrier frequencies. (Note that each carrier is modulated with the same modulation and this is also the case with other forms of modulation considered in this paper.) In a realistic scenario of the legacy LTE Band 8, the Tx band spans 925–960 MHz with 5-MHz-wide channels, and the Rx band spans 880–915 MHz. Carriers of frequencies $f_1 =$ 932.5 MHz and $f_2 =$ 957.5 MHz are in two nonadjacent Tx channels separated by the guard channels. The frequency of the modulating baseband sinewave is $f_m =$ 1 MHz, and power of the input Tx signal is 43 dBm per active channel, so that the total input transmit power is 46 dBm. The modulation frequency f_m and index, $m_a = 0.1$, were chosen to ensure that the modulated carrier signal remained in its respective channel. The TLDN has an electrical length of 720° at 945.0 MHz and the nonlinearity of each section is described by the polynomial model (2).

The spectrum of the signal $\hat{y}(t)$ at the output of the simulated TLDN is shown in Fig. 8. It is dominated by the virtually undistorted original spectrum of the AM-modulated carriers in the Tx band. The signal spectrum of each transmit channel has the expected two modulation sidebands around each carrier frequency, i.e., upper- and lower-sideband spectral lines. In AM these sidebands are in-phase and are of the same magnitude determined by the modulation index m_a and carrier amplitude A. Signal distortion due to nonlinear effects manifests itself as spectral regrowth around each carrier. Note that the broad spectral spread results from waveform compression in the time domain [31].

Fig. 8 also shows that the output signal contains spectral content above and below the Tx band and particularly in the Rx band. These additional spectral components can be

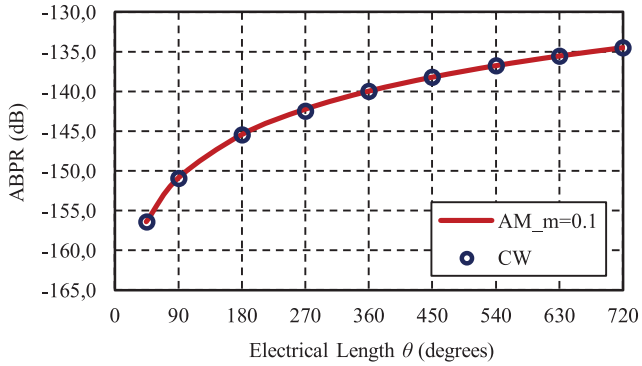

Fig. 9. Simulated ABPR for the two-tone CW and two-carrier AM signals ($m_a = 0.1$).

identified as third-order and fifth-order sideband PIM products. The spectrum centered at Mark 2 contains a large tone at the lower third- and fifth-order IM frequencies of the two input carriers as well as modulation sidebands. Both lower sideband PIM products are inside the Rx band. It is noteworthy that the PIM spectrum has a broader bandwidth than that of the original modulated signals and resembles the spectral regrowth around each of the carriers. (The spectrum associated with the fifth-order mixing products of the carriers appears to be truncated due to insufficient accuracy of the polynomial model (2) deduced from the two-tone CW PIM3 measurements, as mentioned in Section III-B in relation to Fig. 6.)

Engineering intuition of nonlinear behavior in the frequency domain is based on the trigonometric expansion of powers of sums of sinusoids. For discrete tones, the level of the distortion products is used as a metric for characterizing behavior. However, for modulated signals, the appropriate metric is ABPR and calibration is required to gain a qualitative understanding of the impact of PIM for modulated signals.

In Fig. 9, the ABPR due to PIM of the two-carrier AM signal is juxtaposed with that for two-tone CW signals. Here, the two types of input signals have the same mean power and the PIM level is plotted as a function of the electrical length θ of the TLDN. The two curves coincide, thus confirming that even though the spurious spectrum of the output AM test signal is spread across the Rx band, the level of the total PIM down-converted to the Rx band remains almost the same as that for the two-tone CW signal. (The small amount of fifth-order PIM power outside the Rx band has little effect.) Thus the conventional two-tone CW PIM test provides an accurate estimate of PIM interference in the Rx band (i.e., cross-band PIM distortion) for a two-carrier AM signal.

B. Phase-Modulated (PM) Signals

A PM two-carrier signal has the form

$$x(t) = A[\cos(\omega_1 t + m_p \sin(\omega_m t)) + \cos(\omega_2 t + m_p \sin(\omega_m t))] \tag{9}$$

with the same modulating and carrier frequencies and signal power as for the previously considered case of two-carrier AM signal. The distinct characteristics of a PM signal are the

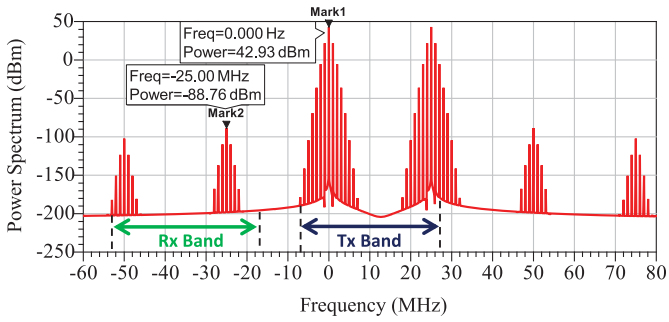

Fig. 10. Two-carrier PM signal spectrum at the TLDN output simulated for $m_p = 1$. The chart center (Mark 1) is at 932.5 MHz.

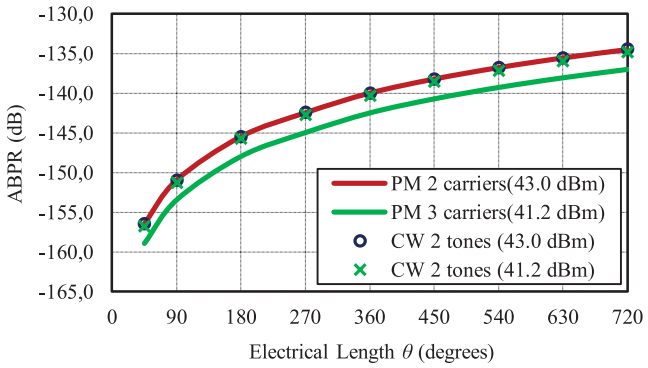

Fig. 11. Simulated ABPR for two-tone CW signals, and two- and three-carrier PM signals ($m_p = 1$) at the respective power per carrier given in the legend.

infinite extent of its spectrum and the out-of-phase sidebands. This is in contrast to the sidebands of an AM modulated signal which are in-phase. With a phase modulation index $m_p < 0.5$, referred to as narrowband PM, the signal spectrum can be reasonably truncated to the two innermost sidebands and the magnitude of the spectrum then resembles that of AM signals. However, in contrast to AM modulation, the number of discernible sidebands increases with m_p. Here, $m_p = 1$ is used to ensure that the discernible power of each modulated carrier remains inside its respective 5 MHz-wide channel.

The output spectrum of the TLDN of length $\theta = 720°$, driven by the two-carrier PM signal with power 43 dBm in each active channel, is shown in Fig. 10. The spectral symmetry of the distorted signal in the Tx band indicates that baseband memory effects, which are known to cause asymmetry, are not important here. This is consistent with the memoryless polynomial model of nonlinearity used and implies negligible phase mismatch of carriers and forward PIM products on the TLDN length.

To assess the impact of PIM on the fidelity of signals appearing in the Rx band, the ABPR of the signal at the output of the line driven by two- and three-carrier PM signals are as shown in Fig. 11, where it is compared with that for a two-tone CW input signals at powers of 43 and 41.2 dBm per channel. The spectral width of each of the distorted PM signals in the Rx band is less than that in the AM two-carrier case, and the ABPR of the output two-carrier PM signal is practically indistinguishable from that of the two-tone CW signal at the

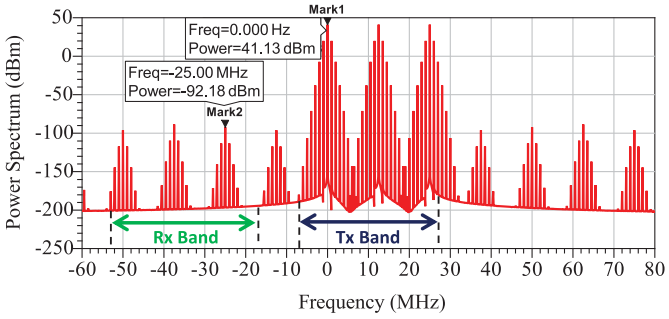

Fig. 12. Three-carrier PM signal spectrum at the TLDN output for $m_p = 1$. The chart center (Mark 1) is at 932.5 MHz.

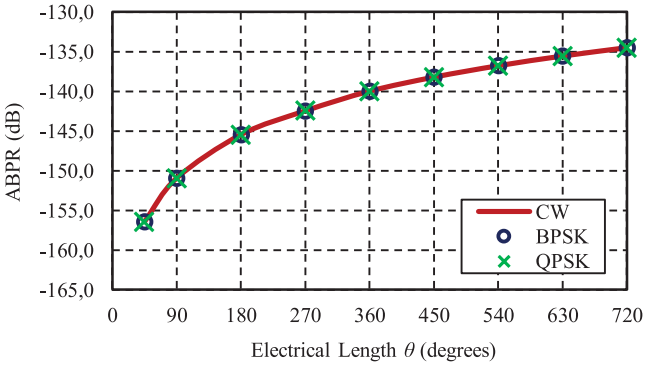

Fig. 13. Simulated ABPR for two-tone CW, two-carrier BPSK and two-carrier QPSK signals transmitted via the TLDN of electrical length θ.

same input power of 43 dBm per carrier. The reduction of the individual carrier powers from 43 to 41.2 dBm results in an ABPR decrease for ~0.36 dB only, which is determined by a PIM3 power growth rate of ~1.2 dB/dB in Fig. 6 instead of the commonly assumed theoretical rate of 3 dB/dB for a discrete nonlinearity (of course, this is prior to saturation effects becoming important).

The important result inferred from Fig. 11 is that ABPR for the PIM-distorted PM signals, as simulated with the aid of the polynomial model (2) derived from two-tone CW PIM3 measurements, agrees with the ABPR for the PIM-distorted discrete CW tones with the same power per carrier. This was also the case with AM signals, and, since AM and PM are representative of analog modulation in general, the reasonable conclusion is that the effect of PIM on analog modulated signals can be accurately predicted using discrete tone characteristics.

The analysis presented here indicates that the ABPR metric adopted for the characterisation of multi-carrier AM and PM signals correlates with the characteristics obtained with discrete CW tones as used in standardized PIM tests. The polynomial model of passive nonlinearity derived from two-tone CW PIM3 measurements can, in principle, enable accurate assessment and prediction of the spectral properties of PIM interference. However, experimental verification for the analog modulated signals is still necessary.

The analysis has been further extended to assess ABPR for the PIM generated by a three-carrier PM signal with carrier frequencies $f_1 = 932.5$ MHz, $f_2 = 945$ MHz and $f_3 = 957.5$ MHz and having 5-MHz channels contained within the Tx bands of E-GSM900 and LTE Band 8 (925 MHz–960 MHz). The power of each carrier in the tests is 41.2 dBm so that the mean total power of the input signal is 46 dBm. The simulated output spectrum with $m_p = 1$ is shown in Fig. 12, and the corresponding ABPR is presented in Fig. 11 as curve "PM 3-carriers (41.2 dBm)". The ABPR of the three-carrier PM signal in Fig. 11 is compared with that of the two-carrier PM signal ("PM 2-carrier (41.2 dBm)") as each carrier has the same power of 41.2 dBm. The ABPR of the three-carrier PM signal is also compared to that of the two-carrier PM signal ("PM 2-carrier (43.0 dBm)") and the 2-tone signal ("CW 2-tone (43.0 dBm)") when all the signals have the same total power of 46.0 dBm.

Two general features are observed. At first, compared with the two-carrier PM case, the three-carrier PM signals produce more combinatorial frequencies, and the PIM products spread more evenly over the adjacent Rx band and beyond. As a result, the peak power of a PIM-induced distortion signal is ~3.5 dB lower than in the two-tone CW case (see Figs. 10 and 12). Second, even though more PIM products are generated with the three-carrier PM signals, the total PIM power in the Rx band is smaller than in the two-tone CW case. This results in the ABPR for the three-carrier PM signal being ~2.5 dB lower than for the two-carrier PM signal with the same power per carrier, see Fig. 11. Thus, it is reasonable to suggest that the standard two-tone CW PIM3 test provides a conservative assessment of PIM interference resulting from multi-carrier analog-modulated signals, and the overestimate may increase with the number of active channels.

C. Digitally Modulated Signals

To quantify effect of PIM from a microstrip TLDN with digitally modulated signals, the analysis was extended to BPSK and QPSK modulated two-tone CW carriers each having a power of 43 dBm for a total power of 46 dBm. The ABPRs simulated for these signals are shown in Fig. 13 in comparison with that of a two-tone CW signal. The ABPR calculation accounts for the PIM products in the Rx band resulting from one symbol in each of the active Tx channels. The total interference power generated in the Rx band by the digitally modulated signals is the same as for the two-tone CW signal.

To elucidate the effect of PIM on received symbols, the constellation diagrams of a QPSK received signal of power −70 dBm were simulated for the cases of additive white Gaussian nose (AWGN) and/or PIM generated in the Rx band. The PIM interference results from a two-carrier QPSK signal of 46 dBm total power transmitted through the 720° long TLDN. The two-carrier signal in the Tx band is defined as before. The AWGN in the Rx band is set to provide the same mean spurious power over the Rx band as that generated by the two-carrier QPSK transmit signal. The resulting constellation diagrams of the intended received signal are shown in Fig. 14. The symbol rates of each transmitted and received signal are the same. It is evident from Fig. 14 that the PIM interference in the Rx band cause correlated distortion of the received

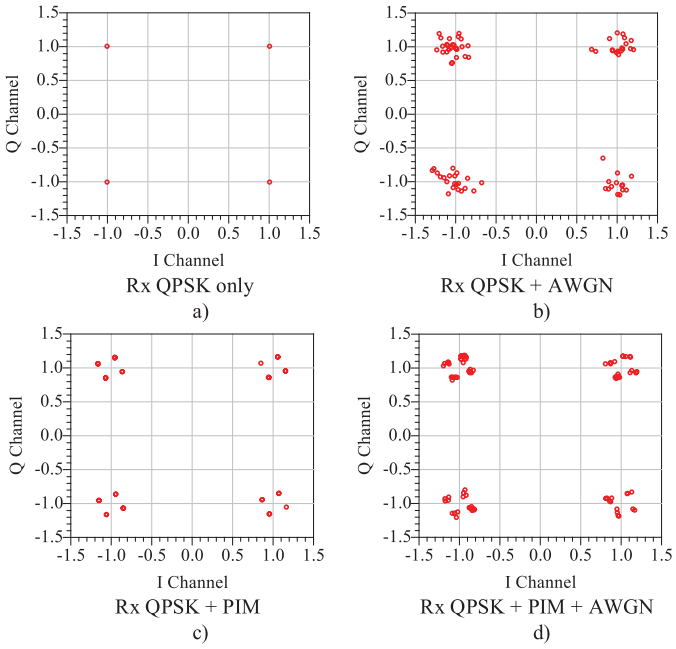

Fig. 14. Simulated constellation diagrams of the received QPSK signal in the presence of AWGN and PIM interference generated by 46-dBm two-carrier QPSK signal transmitting through the test TLDN.

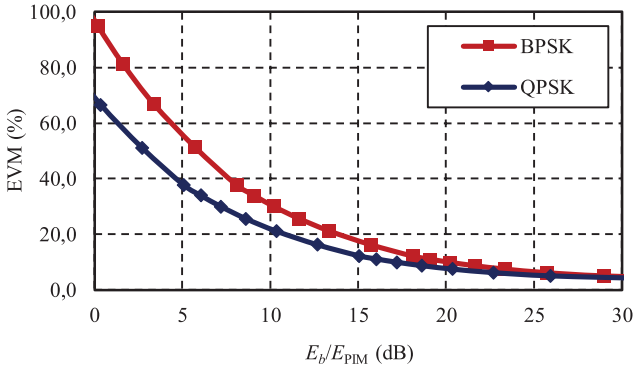

Fig. 15. Simulated EVM for BPSK and QPSK signals versus E_b/E_{PIM}.

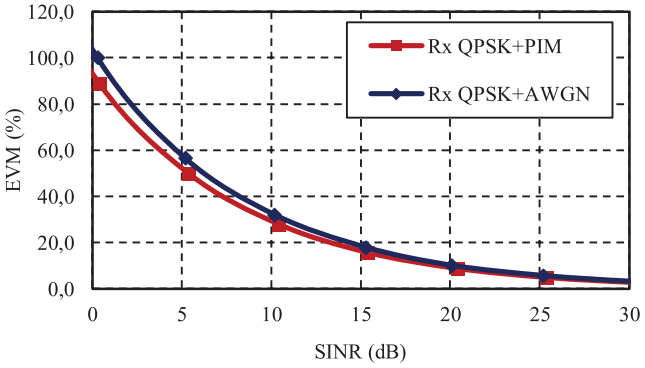

Fig. 16. Simulated EVM for Rx QPSK signal when the Rx distortion is caused by either AWGN or PIM interference.

QPSK signal, and the constellation diagrams reveal the following characteristic features.

1) PIM products decompose each symbol of the received QPSK signal into a quadruple, i.e., the transmitted signal modulation is superimposed on the received signal.
2) Clockwise rotation of each quadruple around its center occurs, as the signal to interference ratio decreases.
3) The quadruple is skewed to a parallelepiped with unequal sides at lower signal to interference ratios.

Indeed, such signal distortions may cause deleterious symbol aliasing, especially in higher order modulation schemes. To assess fidelity of digitally modulated signals, the error-vector magnitude (EVM) is the most commonly used metric. In essence, the EVM is a measure of the symbol constellation deviation from the ideal one due to signal distortion and impairments [32]. It is defined as

$$\mathrm{EVM} = \sqrt{\frac{P_{\mathrm{error}}}{P_{\mathrm{ref}}}} \tag{10}$$

where P_{error} is the rms power of the error vector and P_{ref} is the average ideal reference vector power.

To assess the impact of passive nonlinearity in the transmit chain on received signals, the EVM was evaluated for different modulation types and signal to interference ratios. Fig. 15 shows the EVM for the PIM distorted received signals of two types: 1) BPSK and 2) QPSK modulated two-tone CW carriers of total power of 46 dBm transmitted through the 720° long TLDN. The EVM has been simulated versus the ratio E_b/E_{PIM} where E_b is energy per bit of the received signal and E_{PIM} is PIM energy generated in the Rx band by one bit per active channel transmit Tx signal. It illustrates how EVM decreases when the Rx signal power per symbol increases from −90 dBm to −60 dBm.

Fig. 15 shows that for any chosen value of EVM, the received QPSK signal has less energy per bit than the BPSK signal, and the difference is larger at low power. This is directly related to the fact that the QPSK signal has lower energy per bit than the BPSK signal with the same energy per symbol, i.e., one-bit-per-channel QPSK signal in the Tx band generates lower PIM in the Rx band. Thus E_b and E_{PIM} are smaller for a QPSK signal than for a BPSK signal at the same energy per symbol of the received and transmitted signals whilst their ratio E_b/E_{PIM} may be higher at the fixed energy per symbol of the transmitted and received signals. However, the results of Fig. 15 do not allow us to judge whether QPSK modulation is more resilient to PIM interference than BPSK because the QPSK encodes two bits per symbol and, as such, the PIM contribution per symbol will effectively double.

Finally, it is instructive to estimate the EVM of QPSK signals in the presence of AWGN and PIM interference in the Rx band. The EVM, simulated with respect to the signal to interference plus noise ratio (SINR) at equal AGWN and PIM power levels is shown in Fig. 16 as the Rx signal power level varies from −90 dBm to −60 dBm. At SINR = 0 dB, the EVM with AWGN is ∼10% higher than that for PIM interference, but their difference gradually decreases at higher SINR. However, taking into account that the PIM level in the Rx band may significantly exceed AGWN level,

PIM interference may have strong impact on the fidelity of the received signals. Therefore, the distinctive correlation properties of PIM products should be exploited for mitigation of PIM distortion of the received signals.

V. Conclusion

The objective of this work was to explore the characteristics of PIM generated by distributed passive nonlinearities of a transmission line and characterize the impact of PIM in terms of fidelity metrics for analog and digitally modulated signals in the receive path of an RF front-end. Since the physical origin of PIM is not known in all cases, a behavioral model was adopted for the investigations. It was shown that a polynomial nonlinear model of a short subsection of transmission line accurately modelled PIM when it was cascaded to model the distributed nonlinearity of a microstrip transmission line. This was demonstrated by comparing measured and simulated PIM for a two-tone CW signal for various power levels. The cascaded model was scalable with transmission line length and here was used to determine the effect of line length on PIM. A closed-form transfer function was obtained which mapped an input two-carrier modulated signal at one end of the transmission line to waveform and spectrum at the output of the line. This enabled explicit evaluation of spectral components, and thus PIM-induced interference adequately described by the nonlinearity of the transmission line itself, and predicted the cumulative growth of forward PIM level with line length.

The impact of PIM with analog and digitally modulated signals was explored by implementing the polynomial model in the ADS Circuit Envelope solver environment. Using circuit-envelope analysis, spectral regrowth caused by PIM of modulated carriers and the ABPR and, for digitally modulated signals, EVM metrics for PIM interference in the receive band were determined and compared with interference with discrete tone signals. It was shown that the ABPR of PIM3 interference for two-carrier AM and PM signals is practically indistinguishable from that for a two-tone CW signal. At the same time, it was found that ABPR for the three-carrier PM signal appeared to be considerably lower than that for the two-tone CW signal at the same power per carrier. It was found that the standard two-tone CW PIM3 test provides a conservative estimate of PIM interference in the receive band generated by multicarrier modulated transmitted signals. One of the surprising results is that, because of the small relative growth in phase difference between carriers centered at different frequencies, PIM distortion results in asymmetrical regrowth of output PIM interference for modulated signals.

The effect of PIM interference, characterized by distortion on a constellation diagram and EVM metrics, with two-carrier digitally modulated BPSK and QPSK signals input to a microstrip line was compared with that with AWGN. The EVM for PIM3 interference was lower than that for AWGN of equivalent power. It was argued that this was because PIM interference results in correlated distortion of the received signal when, as usual, the symbol rate of PIM interference and received signals are the same. This implies that PIM interference should not be treated as noise and there is a likely possibility that design strategies can be developed to mitigate the effect of PIM interference on receive signals. Therefore, advanced behavioral and physical models of distributed passive nonlinearities could enable more elaborate assessment and mitigation of the effect of PIM on distortion of digitally modulated signals in multicarrier communications systems.

Appendix

A. Transfer Function for Polynomial Nonlinearity

An explicit form of the TF can be obtained by substituting the input waveform (1) in the polynomial model (2).

Let us consider a passive weakly nonlinear device shown schematically in Fig. 2. Its TF maps an input two-carrier modulated signal $x(t)$ onto the output waveform $y(t)$, which contains the carrier harmonics and combination IM frequencies. The input signal can be represented in the form

$$\begin{aligned} x(t) &= A_1(t)\cos(\omega_1 t + \theta_1(t)) + A_2(t)\cos(\omega_2 t + \theta_2(t)) \\ &= \frac{1}{2}[z_1(t)\mathrm{e}^{j\omega_1 t} + {z_1}^*(t)\mathrm{e}^{-j\omega_1 t}] \\ &\quad + \frac{1}{2}[z_2(t)\mathrm{e}^{j\omega_2 t} + {z_2}^*(t)\mathrm{e}^{-j\omega_2 t}] \end{aligned} \tag{A1}$$

where $z_{1,2}(t) = A_{1,2}(t)\exp\{j\theta_{1,2}(t)\}$ are the baseband complex envelopes of the modulated carriers. The terms of (2) can be expressed using the binomial expansion

$$x^{2n+1}(t) = \frac{1}{2^{2n+1}}\left[\begin{array}{c} z_1(t)\mathrm{e}^{j\omega_1 t} + {z_1}^*(t)\mathrm{e}^{-j\omega_1 t} \\ + z_2(t)\mathrm{e}^{j\omega_2 t} + {z_2}^*(t)\mathrm{e}^{-j\omega_2 t} \end{array}\right]^{2n+1}. \tag{A2}$$

In the simplest case $z_1(t) = z_2(t) = z(t)$, we have

$$\begin{aligned} x^{2n+1}(t) &= \frac{1}{2^{2n+1}}\left[z^*(t)\right]^{2n+1}(\mathrm{e}^{-j\omega_1 t} + \mathrm{e}^{-j\omega_2 t})^{2n+1} \\ &\quad \times \sum_{k=0}^{2n+1}\binom{2n+1}{k}\frac{[z(t)]^k(\mathrm{e}^{j\omega_1 t} + \mathrm{e}^{j\omega_2 t})^k}{[z^*(t)]^k(\mathrm{e}^{-j\omega_1 t} + \mathrm{e}^{-j\omega_2 t})^k}. \end{aligned} \tag{A3}$$

Substituting (A3) into (2) gives

$$\begin{aligned} y(t) &= \sum_{n=0}^{(N-1)/2}\sum_{k=0}^{2n+1}\binom{2n+1}{k}\frac{a_{2n+1}\left[z^*(t)\right]^{2n+1-k}[z(t)]^k}{2^{2n+1}} \\ &\quad \times(\mathrm{e}^{j\omega_1 t} + \mathrm{e}^{j\omega_2 t})^k(\mathrm{e}^{-j\omega_1 t} + \mathrm{e}^{-j\omega_2 t})^{2n+1-k} \\ &= \sum_{n=0}^{(N-1)/2}\sum_{k=0}^{2n+1}\binom{2n+1}{k}\frac{a_{2n+1}\left[z^*(t)\right]^{2n+1-k}[z(t)]^k}{2^{2n+1}} \\ &\quad \times\sum_{q=0}^{k}\sum_{p=0}^{n-k}\binom{k}{q}\binom{2n+1-k}{p} \\ &\quad \times \mathrm{e}^{j[(q-p)\omega_1 + (2k-2n-1-q+p)\omega_2]t}. \end{aligned} \tag{A4}$$

The odd-order terms in (A4) satisfy the following conditions:

$$\omega_l = (l+1)\omega_1 - l\omega_2 \tag{A5}$$

where $l = (M-1)/2$, and $|M|$ is the order of the IM products: $M = \pm 3, \pm 5, \ldots, N$. Substituting (A5) into (A4) gives

$$\begin{cases} q - p = l + 1 \\ 2k - 2n - 1 - q + p = -l \end{cases}. \tag{A6}$$

Hence

$$k = n + 1. \tag{A7}$$

Substituting (A7) into (A4) and retaining only the carrier frequencies and the IM products nearby the carrier frequencies, we obtain the output band-limited response at fundamental and odd-order IM frequencies as

$$\begin{aligned} \tilde{y}(t) = z(t) &\sum_{n=0}^{(N-1)/2} \frac{a_{2n+1}}{2^{2n+1}} \binom{2n+1}{n+1} |z(t)|^{2n} \sum_{q=0}^{n+1} \sum_{p=0}^{n} \binom{n+1}{q} \\ &\times \binom{n}{p} e^{j[(q-p)\omega_1 + (1-q+p)\omega_2]t} \\ &= \mathrm{Re}\left\{ \sum_{\substack{M=-N \\ M-odd}}^{N} y_M(t) e^{j[\omega_1 (M+1)/2 + \omega_2 (1-(M+1)/2)]t} \right\} \end{aligned} \tag{A8}$$

where

$$\begin{aligned} y_M(t) = e^{j\theta(t)} &\sum_{n=0}^{(N-1)/2} \frac{a_{2n+1}}{2^{2n+1}} \binom{2n+1}{n+1} [A(t)]^{2n+1} \\ &\times \sum_{k=(M+1)/2}^{n+1} \binom{n+1}{k} \binom{n}{k - \frac{M+1}{2}}. \end{aligned} \tag{A9}$$

B. Measurement Setup

Full details of the PIM measurements have been reported elsewhere, see, e.g., [25] and references therein. The specimens fabricated on the Taconic RF laminate comprised three replicas of 50-Ω uniform microstrip transmission line (see Fig. 17). To ensure the return loss in the Tx and Rx bands better than 20 dB, the microstrip lines were fitted with custom designed low-PIM cable launchers. The launchers were made of the PIM certified cable assemblies with DIN 7/16 connectors cut in halves and tinplated solid copper transition units at the open ends. The cables were soldered to the signal track and ground plane of microstrip line with Sn40/Pb60 solder. The measurements were carried out in anechoic chamber with the aid of a commercial two-port PIM analyser Summitek SI-900B. The acquired data were averaged over the triplet of identical lines and five measurements to reduce the effect of carrier power variations and fabrication tolerances. The obtained data were used for the model extraction.

C. Polynomial Coefficients

Table I lists the polynomial coefficients retrieved from the power sweep PIM3 measurements of the $L_0 = 914$ mm microstrip line.

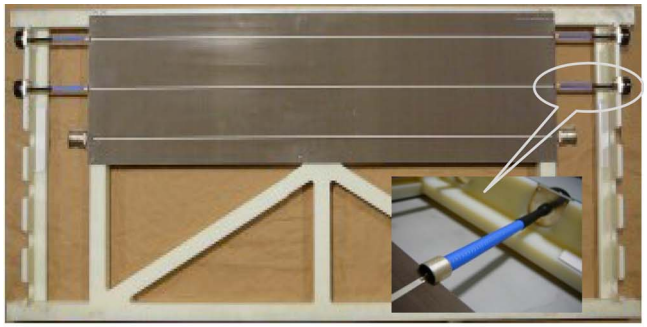

(a)

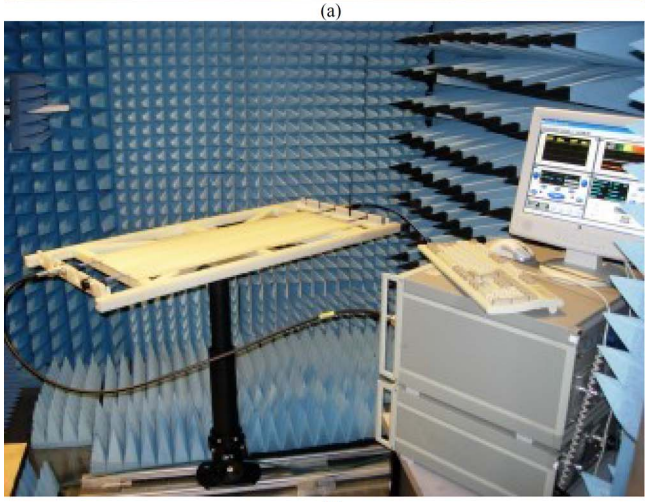

(b)

Fig. 17. Two-port measurements of PIM on microstrip lines. (a) PCB specimen containing three replicas of 50 Ohm microstrip lines in the test fixture; the low-PIM cable launcher with coaxial to microstrip transition is shown in insert; (b) the test PCB connected to the Summitek SI-900B PIM analyzer in anechoic chamber.

TABLE I

POLYNOMIAL COEFFICIENTS RETRIEVED FROM THE POWER SWEEP PIM3 MEASUREMENTS OF $L_0 = 914$ mm MICROSTRIP LINE

Term a_n	Value ($V^{(1-n)}$)
a_1	1
a_3	6.60E-09
a_5	-2.54E-11
a_7	4.95E-14
a_9	-5.50E-17
a_{11}	3.76E-20
a_{13}	-1.65E-23
a_{15}	4.71E-27
a_{17}	-8.76E-31
a_{19}	1.02E-34
a_{21}	-6.75E-39
a_{23}	1.94E-43

ACKNOWLEDGMENT

The authors would like to thank Dr. E. Doumanis and V. Venkateswaran, Alcatel-Lucent's Bell Labs, for fruitful discussions.

REFERENCES

[1] R. Butler, A. Kurochkin, and N. Hugh, "Intermodulation products of LTE and 2G signals in multitechnology RF paths," *Bechtel Commun. Techn. J.*, vol. 2, no. 1, pp. 1–12, Dec. 2009.

[2] J. R. Wilkerson, K. G. Gard, A. G. Schuchinsky, and M. B. Steer, "Electro-thermal theory of intermodulation distortion in lossy microwave components," *IEEE Trans. Microw. Theory Techn.*, vol. 56, no. 12, part 1, pp. 2717–2725, Dec. 2008.

[3] *Passive r.f. and Microwave Devices, Intermodulation Level Measurement—Part 1: General Requirements and Measuring Methods*, IEC 62037–12012.

[4] D. Weinstein, "Passive intermodulation distortion in connectors, cable and cable assemblies," in *White Paper XP002330778*, 2001, pp. 1–9.

[5] J.-J. DeLisle, "New modulation schemes raise PIM," *Microw. & RF*, vol. 53, no. 3, pp. 36–40, Mar. 2014.

[6] R. Butler, "PIM testing: advanced wireless services emphasize the need for better PIM control," *COMMSCOPE White Paper WP-107482-EN (2/14)*, pp. 1–10, 2014.

[7] "Understanding PIM," in *Applicant. Notes*, Anritsu Co. [Online]. Available: http://www. anritsu.com

[8] K. M. Gharaibeh, K. G. Gard, and M. B. Steer, "Estimation of co-channel nonlinear distortion and SNDR in wireless systems," *IET Microw. Antennas Propag.*, vol. 1, no. 5, pp. 1078–1085, 2007.

[9] J. W. Boyhan, H. F. Lenzing, and C. Koduru, "Satellite passive intermodulation: systems considerations," *IEEE Trans. Aerosp. Electron. Syst.*, vol. 32, no. 3, pp. 1058–1064, Jul. 1996.

[10] P. M. Cabral, J. C. Pedro, and N. B. Carvalho, "Modelling nonlinear memory effects on the AM/AM, AM/PM and two-tone IMD in microwave PA circuits," *Int. J. RF Microw. Comput.-Aided Eng.*, vol. 16, no. 1, pp. 13–23, Jan. 2006.

[11] D. Kozlov, A. Shitvov, and A. Schuchinsky, "On passive intermodulation test of analog and digital systems," in *Proc. Int. Workshop Integr. Nonlinear Microw. Millimetre-Wave Circuits*, Taormina, Italy, Oct. 1–2, 2015, pp. 1–3.

[12] B. A. Auld, M. Didomenico Jr., and R. H. Pantell, "Traveling-wave harmonic generation along nonlinear transmission lines," *J. Appl. Phys.*, vol. 33, pp. 3537–3545, Dec. 1962.

[13] A. P. Foord and A. D. Rawlins, "A study of passive intermodulation interference in space RF Hardware," ESTEC, Univ. of Kent at Canterbury, Contract 111036, Final Rep, 1992.

[14] D. Seron, C. Collado, J. Mateu, and J. M. O'Callaghan, "Analysis and simulation of distributed nonlinearities in ferroelectrics and superconductors for microwave applications," *IEEE Trans. Microw. Theory Techn.*, vol. 54, no. 3, pp. 1154–1160, Mar. 2006.

[15] J. Mateu *et al.*, "Third-order intermodulation distortion and harmonic generation in mismatched weakly nonlinear transmission lines," *IEEE Trans. Microw. Theory Techn.*, vol. 57, no. 1, pp. 10–18, Jan. 2009.

[16] D. E. Zelenchuk, A. P. Shitvov, A. G. Schuchinsky, and V. F. Fusco, "Passive intermodulation in finite lengths of printed microstrip lines," *IEEE Trans. Microw. Theory Techn.*, vol. 56, no. 11, part 1, pp. 2426–2434, Nov. 2008.

[17] J. R. Wilkerson, P. G. Lam, K. G. Gard, and M. B. Steer, "Distributed passive intermodulation distortion on transmission lines," *IEEE Trans. Microw. Theory Techn.*, vol. 59, no. 5, pp. 1190–1205, May 2011.

[18] D. Kozlov, A. Shitvov, and A. Schuchinsky, "Characterisation of passive intermodulation in passive RF devices with X-parameters," in *Proc. Loughborough Antennas and Propag, Conf.*, Loughborough, U.K., Nov. 2014, pp. 64–67.

[19] J. Sombrin, "Non-analytic at the origin, behavioural models for active or passive non-linearity," *Int. J. Microw. Wireless Techn.*, vol. 5, no. 2, pp. 133–140, 2013.

[20] A. Ignea and A. De Sabata, "Hysteresis distortions for two-tone signals," in *Proc. 15th IMEKO TC 4 Symp. Int. Meas. Confederation Techn. Committee 4 Symp.*, Iasi, Romania, 2007, pp. 1–5.

[21] A. Ignea and R. Körtvelyessy, "Modeling of the passive intermodulation in Transmission Lines," in *Proc. 9th Int. Symp. Design and Technol. Electron. Packaging*, Timişoara, Romania, Sep. 2003, pp. 27–30.

[22] C. D. Bond, C. S. Guenzer, and C. A. Carosella, "Intermodulation generation by electron tunnelling through aluminum-oxide films," *Proc. IEEE*, vol. 67, no. 12, pp. 1643–1652, Dec. 1979.

[23] *Unwanted Emissions in the Out-of-Band Domain*, Recommendation ITU-R SM.1541–62015, pp. 1–33.

[24] P. Amb, F. Launa, J. M. Foumier, and J. C. Grasset, "A simple RF power amplifier characterization using AM-AM, AM-PM measurements based on CDMA signal statistics," in *Proc. 34th Eur. Microw. Conf.*, Amsterdam, The Netherlands, 2004, pp. 693–696.

[25] A. Shitvov, D. Zelenchuk, and A. Schuchinsky, "Carrier-power dependence of passive intermodulation products in printed lines," in *Proc. Loughborough Antennas and Propag, Conf.*, Loughborough, U.K., Nov. 2009, pp. 177–180.

[26] A. P. Shitvov, D. E. Zelenchuk, A. G. Schuchinsky, and V. F. Fusco, "Passive intermodulation in printed lines: Effects of trace dimensions and substrate," *IET Microw. Antennas Propag.*, no. 3, pp. 260–268, Mar. 2009.

[27] D. Kozlov, A. Shitvov, and A. Schuchinsky, "Passive intermodulation in distributed circuits with cascaded discrete nonlinearities," in *Proc. 9th Eur. Conf. Antennas and Propag.*, Lisbon, Portugal, Apr. 13–17, 2015, pp. 1–5.

[28] D. E. Root, J. Verspecht, J. Horn, and M. Marcu, *X-Parameters: Characterization, Modeling, and Design of Nonlinear RF and Microwave Components*. Cambridge, U.K.: Cambridge Univ., 2013.

[29] J. C. Pedro and N. B. Carvalho, *Intermodulation Distortion in Microwave and Wireless Circuits*. Norwood, MA, USA: Artech House, 2002.

[30] J. R. Wilkerson, I. M. Kilgore, K. G. Gard, and M. B. Steer, "Passive intermodulation distortion in antennas," *IEEE Trans. Antennas Propag.*, vol. 63, no. 2, pp. 474–482, Feb. 2015.

[31] M. B. Steer, *Microwave and RF Design: A Systems Approach*, 2nd ed. Raleigh, NC, USA: IET/SciTech Publishing, 2014.

[32] R. A. Shafik, S. Rahman, and R. Islam, "On the extended relationships among EVM, BER and SNR as performance metrics," in *Proc. 4th Int. Conf. Electr. Comput. Eng.*, Dec. 2006, pp. 408–411.

Dmitry S. Kozlov (S'16) was born in Borisov, USSR, in 1988. He received the B.S. and M.S. degrees in radiophysics from Saint Petersburg Electrotechnical University, Saint Petersburg, Russia, in 2009 and 2011, respectively.

He is currently the Marie Curie Early Stage Researcher with the Institute of Electronics, Communications and Information Technology (ECIT), Queen's University Belfast, Belfast, U.K.. His primary research focuses are in the area of microwave and antenna theory, including synthesis of antenna arrays, mechanisms of PIM generation in microwave passive, and tunable devices and wireless energy transfer systems.

Alexey P. Shitvov (M'06) received Diploma Engineer degree in semiconductor devices and microelectronics from Nizhny Novgorod State University, Nizhny Novgorod, Russia, in 1995, and the Ph.D. degree in electronics and electrical engineering from the Queen's University Belfast, Belfast, U.K., in 2009.

From 2000 to 2004, he was a Research Assistant with the Department of Electronics, Nizhny Novgorod State University, Nizhny Novgorod, Russia, working on design and simulation of surface acoustic wave devices. From 2009 to 2014 he was a Royal Academy of Engineering Research Fellow with the ECIT Institute, Queen's University Belfast (QUB), Belfast, U.K., conducting research on phenomenology and mitigation of passive intermodulation in communication components and systems. He is currently a Lecturer on millimeter-wave and submillimeter-wave passive and active components and devices with the School of Electronics, Electrical Engineering and Computer Science, QUB. His research interests include accurate characterization and modelling of communication nonlinearities, advanced microwave materials, and millimeter-wave communication and sensing system design under hardware constraints.

Alexander G. Schuchinsky (M'97–SM'05–F'14) received Ph.D. degree in radiophysics from Leningrad Electrotechnical Institute, Leningrad and the academic title of Senior Research Scientist, USSR, in 1983 and 1988, respectively.

He then became a Senior Research Scientist. He was a Leading Scientist with the Microwave Electrodynamics Laboratory, Rostov State University, Russia, and a Chief Engineer with Deltec-Telesystems, New Zealand. During 2002–2015, he was with the School of Electronics, Electrical Engineering and Computer Science, Queen's University of Belfast, Belfast, U.K. He has published three international patents, four book chapters, and over 200 refereed journal and conference papers. His research interests include physics-based modelling of linear and nonlinear phenomena in complex electromagnetic structures, metamaterials, and nonreciprocal devices, passive intermodulation effects, and characterization of electromagnetic materials.

Dr. Schuchinksy was a corecipient of the IEEE 2010 Microwave Prize and received the 2012 V.G. Sologub Award for contribution to Computational Electromagnetics. He was a cofounder and General Co-Chair of the annual conference series "Metamaterials: International Congress on Advanced Electromagnetic Materials in Microwaves and Optics" and is a member of the Board of Directors of the Virtual Institute for Artificial Electromagnetic Materials and Metamaterials, "Metamorphose VI".

Michael B. Steer (S'76–M'78–SM'90–F'99) received the B.E. (Hons.) and Ph.D. degrees from the University of Queensland, Queensland, Qld., Australia, in 1976 and 1983, respectively.

He is currently the Lampe Distinguished Professor of Electrical and Computer Engineering at North Carolina State University (NC State), Raleigh, NC, USA. He has authored more than 470 publications and four books including the textbook *Microwave and RF Design: A Systems Approach* (SciTech, 2010).

Prof. Steer was Secretary of the IEEE Microwave Theory and Techniques Society (MTT-S) in 1997 and was a member of the MTT-S Administrative Committee from 1998 to 2001, and from 2003 to 2006. He is a former editor-in-chief of the IEEE TRANSACTIONS ON MICROWAVE THEORY AND TECHNIQUES. He was the recipient of the Presidential Young Investigator Award in 1986, he was the Jack S. Kilby Lecturer in 2003, and, in 1994 and 1996, he was the recipient of the Bronze Medallion from U.S. Army Research for Outstanding Scientific Accomplishment. In 2007, he received a Distinguished Service Recognition Award from IEEE MTT-S. He received the 2010 Microwave Prize for the best paper on Microwave Engineering in any IEEE publication in the preceding year. In 2011, he received the Distinguished Educator Award from IEEE/ MTT-S, was inducted into the Electronic Warfare Technology Hall of Fame sponsored by the Association of Old Crows, and was named one of the Most Creative Teachers in the South by Oxford American Magazine. In 2013, he received the R.J. Reynolds Award for Excellence in Teaching, Research, and Extension from the College of Engineering at NC State.